

Implementation of PSOANN Optimized PI Control Algorithm for Shunt Active Filter

M. Sujith^{1,*} and S. Padma²

Abstract: This paper proposes the optimum controller for shunt active filter (SAF) to mitigate the harmonics and maintain the power quality in the distribution system. It consists of shunt active filter, Voltage Source Inverter (VSI), series inductor and DC bus and non-linear load. The proposed hybrid approach is a combination of Particle Swarm Optimization (PSO) and Artificial Neural Network (ANN) termed as PSOANN. The PI controller gain parameters of k_p and k_i are optimized with the help of PSOANN. The PSOANN improves the accuracy of tuning the gain parameters under steady and dynamic load conditions; thereby it reduces the values of THD within the prescribed limits of IEEE 519. The PSO optimizes the dataset of terminal voltage and DC voltage present in shunt active filter for different load condition. The optimized dataset acts as the input for the controller to predict the optimal gain with minimal error and to generate the optimized control signal for the SAF. The proposed methodology is modelled and simulated with the help of MATLAB/Simulink platform and illustrated the few test cases considered for exhibiting the performance of proposed hybrid controller. The experimental results are measured with developed laboratory prototype and compared with the simulation results to validate the effectiveness of the proposed control methodology.

Keywords: Artificial neural network, particle swarm optimization, shunt active filter, voltage source inverter, total harmonic distortions.

1 Introduction

The power quality (PQ) issues have become a critical problem in distribution and transmission networks due to the extensive use of power electronics devices. The non-linear loads connected to the power source/grid increases the harmonic content in the utility side. The power system network suffers from disturbance and losses due to the presence of harmonic contents produced by the non-linear loads. The utilization of power electronics-based controllers and non-linear loads lead to low power factor, an increase of neutral current, overheating, generates waveform disturbances in the power system [Terciyani, Avci, Yilmaz et al. (2012); Mikkili and Panda (2012)]. The disadvantage in the fixed compensation technique is due to resonance conditions which are employing as

¹ Department of EEE, IFET College of Engineering, Villupuram, Tamilnadu, 605108, India.

² Department of EEE, Sona College of Engineering, Salem, 636005, India.

* Corresponding Author: M. Sujith. Email: msujitheee@yahoo.co.in.

Received: 23 October 2019; Accepted: 02 January 2020.

different load conditions [Zaveri and Chudasama (2012)]. In addition to the utilization of passive filter, hold only specific harmonic content in the distribution networks [Marzoughi, Imaneini and Moeini (2013)]. The generation of reference current using the component i_d-i_q is presented to compensate for the unbalanced harmonic content [Panda and Mikkili (2013)]. The control strategies are employed to compensate for the current harmonics and selective harmonic elimination to improve the power factor [Usman and Musa (2013)]. The combination of fuzzy logic control and PI are employed to increase the reactive power compensation under various load conditions, thereby improving the filter performance [Patel and Panda (2014)]. The study investigates the performance of filter, voltage imbalance by employing the tuned passive filter along with the active filter [Lee, Wang, Li et al. (2015)]. By considering the different source voltage, the shunt filters are employed to improve the stability and reactive power to update the passive filter [Barghi Latran, Yoldas and Teke (2015)]. The various control strategies have been proposed and validated by the researches, such as reference current theory [Suresh and Singh (2014)], PLL based unit template generation [Patjoshi and Kanta Mahapatra (2013)], synchronous frame theory [Jain, Agarwal, Jain et al. (2016)] for estimation of compensation current. For regulation of DC voltage using the fuzzy logic controller [Yin, Lin, Li et al. (2015)] and artificial neural networks [Roy, Krishna Mandal, Chandra Mandal et al. (2018)] based controllers. Most of the researchers suggested the metaheuristic algorithm to solve the optimization and the gain parameters for PI such as Genetic Algorithm [Parithimar Kalaignan (2015)], gravitational search algorithm [Elsisi, Soliman, Aboelela et al. (2015)], Bacterial Foraging [Mohammadi (2015)], Ant colony optimization [Sakthivel, Vijayakumar, Senthilkumar et al. (2015)], Particle swarm optimization [Letha, Thakur and Kumar (2016)], Differential evolution [Biswas, Suganthan and Amaratunga (2017)], artificial bee colony [Baghaee, Mirsalim, Gharehpetian et al. (2017)] and Grasshopper optimization Algorithm [Barik and Das (2018)] are addressed to reduce the losses by determining the appropriate switching angles for generation of PWM pulses. These algorithms are combined towards the global optimization search for best validation and contrasted during the searching process of optimal parameters. The converging time required for the PSO is small compared to GA. The fitness value computed by PSO is larger, it leads to superior performance. By finding the appropriate values of K_p and K_i , the cost function is minimized. A conventional PI controller is restricted to employed in non-linear control and open loop systems due to lacking in time and tuning process. In the traditional approach, the gain values may not give better performance under various dynamic conditions. In the proposed method the continuous assessment of gain values is employed through the PI controller used in Shunt active filter and also it improves the dynamic performance of the controller. The most of the researchers are inspired with ANN due to the self-learning ability, parallel computing in nature, acceptable performance with trained data and adaptation capability. ANN can deliver fast corrective action, under any distortion condition. The neuron weights are adjusted to lower the value of THD of the source current as per the IEEE standard 519 [Arseneau, Heydt and Kempker (1997)]. In this proposed method, PSOANN approach is employed to reduce the THD level within the prescribed limits of IEEE 519 standards. The PSO algorithm is engaged to generate the optimum data set and ANN method is utilized to reduce the error signal, thereby generating the optimum PWM pulses for the

shunt active filter. The proposed controller has an ability to tune the open loop system and also consume less timing for tuning rather than the conventional PI controller. ANN is preferred mostly amount the researchers due to adoption capability, faster response and satisfactory performance. The trained data is very close to the test data acquired by the artificial neural network. The other methods have premature convergence problem compared to Particle swarm optimization (PSO). The combination of PSO and ANN doesn't cause specific damage in optimization process but it takes more execution time and ability to compute in single optimization process. Section II covers the system descriptions. Section III delineates the proposed PGOANN controller. Section IV depicts the simulation results and verification of the proposed method.

2 System descriptions

The proposed control system for Shunt Active Filter (SAF) is depicted in Fig. 1. The proposed structure consists of an active filter, voltage regulator, Point of common coupling (PCC), non-linear load, filter inductance and resistance, three phase PWM and DC voltage bus. The SAF is connected to the PCC through filter resistance and inductances for mitigating the current harmonic components. No need of additional components required for filtering the ripple contents generated by the inverter due to the high impedance of LC filter connected to the PCC. The diode bridge rectifier and R_L load are employed as non-linear load to test the system performance.

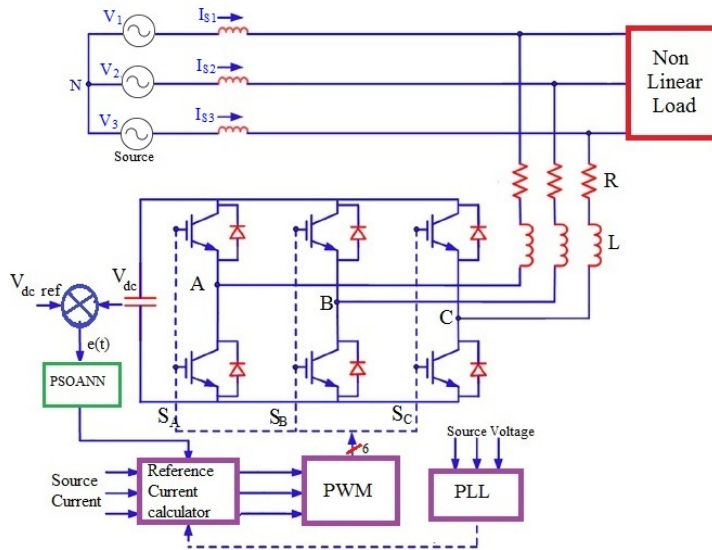


Figure 1: Schematic diagram of PSOANN based Shunt active filter

2.1 Mathematical modelling of SAF

The Shunt active filter is mathematically modeling by the kirchoff's law in terms of differential equations expressed as

$$V_{sy} = L_{HF} \frac{dI_{FC}}{dt} + R_{HF} I_{FCy} + V_{CRFy} + V_{My} + V_{NF} \tag{1}$$

$$I_{FCy} = C_{RF} \frac{dV_{CRFy}}{dt} \quad (2)$$

$$\frac{dV_{dc}}{dt} = \frac{1}{C_{dc}} I_{dc} \quad (3)$$

Assumption to be made in this analysis (i) Absence of zero sequence current and (ii) Balanced AC supply voltage.

Three phase supply voltage is given by

$$V_{S1} + V_{S2} + V_{S3} = 0 \quad (4)$$

Three phase supply current is formulated by

$$I_{S1} + I_{S2} + I_{S3} = 0 \quad (5)$$

The voltage between the supply neutral and active filter is formulated by sub $y=1,2$ and 3 in (1)

$$V_{NF} = -\frac{1}{3} \sum_{y=1}^3 V_y M \quad (6)$$

The switching functions (C_s) of the inverter is formulated by

$$C_s = \begin{cases} 1, & \text{if } S_s \text{ is on and } S'_s \text{ is off} \\ 0, & \text{if } S_s \text{ is off and } S'_s \text{ is on} \end{cases} \quad (7)$$

The dynamic model of the filter is expressed as

$$\frac{dI_{cy}}{dt} = \frac{R_{HF}}{L_{HF}} I_{Cy} - \frac{V_{CRFy}}{L_{HF}} - \frac{1}{L_{HF}} \left(C_y - \frac{1}{3} \sum_{y=1}^3 C_y \right) V_{dc} + \frac{V_{sy}}{L_{HF}} \quad (8)$$

The function of the switching state is given by the equation

$$q_{my} = \left(C_y - \frac{1}{3} \sum_{y=1}^3 C_y \right) \quad (9)$$

where $m=0$ or 1 .

The model of SAF in three phase reference frame is denoted by the equation

$$L_{HF} \frac{d^2 I_{C1}}{dt^2} = R_{HF} \frac{dI_{C1}}{dt} - \frac{1}{C_{HF}} I_{C1} - q_{m1} \frac{dV_{dc}}{dt} + \frac{dV_{s1}}{dt} \quad (10)$$

$$L_{HF} \frac{d^2 I_{C2}}{dt^2} = -R_{HF} \frac{dI_{C2}}{dt} - \frac{1}{C_{HF}} I_{C2} - q_{m2} \frac{dV_{dc}}{dt} + \frac{dV_{s2}}{dt} \quad (11)$$

The transformed model is obtained through SRF is represented by the equations

$$\frac{dV_{dc}}{dt} = \frac{q_{md}}{c_{dc}} I_d + \frac{q_{mq}}{C_{dc}} I_q \quad (12)$$

$$\frac{dV_{CHFd}}{dt} = \frac{1}{C_{HF}} I_d + \omega V_{CRFq} \quad (13)$$

$$\frac{dV_q}{dt} = \frac{1}{C_{HF}} I_q - \omega V_{CRFd} \quad (14)$$

The switching functions for the steady-state are given as

$$D_{nd} = \frac{L_{HF}}{V_{dc}^*} \left[-\frac{dI_d^*}{dt} - \frac{R_{HF}}{L_{HF}} I_d^* + \omega I_q - \frac{V_{CHFd}^*}{L_{HF}} + \frac{1}{L_{HF}} V_{sd} \right] \quad (15)$$

$$D_{nq} = \frac{L_{HF}}{V_{dc}^*} \left[-\frac{dI_q^*}{dt} - \frac{R_{HF}}{L_{HF}} I_q^* - \omega I_d - \frac{V_{CHFq}^*}{L_{HF}} + \frac{1}{L_{HF}} V_{sq} \right] \quad (16)$$

The supply currents (I_{S1} , I_{S2} , I_{S3}) and supply voltage (V_{S1} , V_{S2} , V_{S3}) and V_{dc} of the inverter are employed to generate the appropriate PWM signal for the VSI. The values of I_d and I_q are extracted from the supply currents is formulated by the equation

$$\begin{bmatrix} I_d \\ I_q \\ I_0 \end{bmatrix} = \frac{2}{3} \begin{bmatrix} \sin(\omega_s t) & \sin(\omega_s t - 2\pi/3) & \sin(\omega_s t + 2\pi/3) \\ \cos(\omega_s t) & \cos(\omega_s t - 2\pi/3) & \cos(\omega_s t + 2\pi/3) \\ 1/\sqrt{2} & 1/\sqrt{2} & 1/\sqrt{2} \end{bmatrix} \begin{bmatrix} I_{S1} \\ I_{S2} \\ I_{S3} \end{bmatrix} \quad (17)$$

The values of reference currents I_d and I_q are decomposed and equated as

$$\begin{bmatrix} I_d \\ I_q \end{bmatrix} = \begin{bmatrix} I_{dDC} \\ I_{qDC} \end{bmatrix} + \begin{bmatrix} I_{dAC} \\ I_{qAC} \end{bmatrix} \quad (18)$$

Later, the reference frame currents are calculated as follows

$$\begin{bmatrix} I_{S1} \\ I_{S2} \\ I_{S2} \end{bmatrix} = \begin{bmatrix} \sin(\omega_s t) & \cos(\omega_s t) \\ \sin(\omega_s t - 2\pi/3) & \cos(\omega_s t - 2\pi/3) \\ \sin(\omega_s t + 2\pi/3) & \cos(\omega_s t + 2\pi/3) \end{bmatrix} \begin{bmatrix} I_d^* \\ I_q^* \end{bmatrix} \quad (19)$$

The reference voltage is obtained from the equation,

$$V_S^* = K_V I_S \quad (20)$$

The gain parameter (k_v) is depending on the response of the voltage and damping factor defined as k_p and k_i . The gain parameters are obtained through the proposed optimization algorithm. The approach of PSOANN is clearly delineated in the following section.

3 PSOANN based prediction of gain parameters

The PI gain parameters are optimized with the help of PSO and ANN method are shown in Fig. 2. This method enhances the accuracy of parameter prediction in SAPF. The PSOANN is employed to generate the optimum PWM pulses for the inverter. The accurate optimal solution is obtained by executing the PSO algorithm for the maximum

number of iterations. The output of the particle swarm optimization (PSO) is acting as the input for the artificial neural network (ANN) controller for predicting the exact PWM pulse with minimum error tolerance. The observation of the approach shows that the harmonic distortion is minimized in the distribution network.

3.1 PSO for dataset generation

The particle swarm optimization is initiated with a group of random variables and then searches for the optimal solutions (19). In each iteration, PSO updates the generation by two best values. The first one is the best solutions (fitness) it is termed as P_{best} and the iterated value is stored. The second-best value is termed as global best value g_{best} , it is tracked by the optimizer.

The value of the k^{th} particle is represented by $x_k=(x_{k1}, x_{k2}, \dots, x_{kd})$ in the d -dimensional space. Recorded value is represented by the equation

$$P_{best} = (P_{bestk1}, P_{bestk2}, \dots, P_{bestkd}) \tag{21}$$

The best particle is identified in the global is termed as g_{bestd} . The velocity of the k^{th} particle is represented by

$$V_k=(V_{k1}, V_{k2}, \dots, V_{kd}) \tag{22}$$

The current velocity is used to calculate the modified position and velocity of each particle. Then the distance is calculated from P_{bestkd} to g_{bestd} is formulated by the equation,

$$v_{k,m}^{(t+1)} = wv_{k,m}^{(t)} + c_1rand() (P_{bestk,m} - x_{k,m}^{(t)}) + c_2rand() (g_{bestk,m} - x_{k,m}^{(t)}) \tag{23}$$

$$x_{k,m}^{(t+1)} = x_{k,m}^{(t)} + v_{k,m}^{(t+1)} \tag{24}$$

The optimum solutions are computed with the help of PSO with minimal error and then the system is engaged to choose the appropriate gain parameters.

$$X_i = \begin{bmatrix} k_p^{11} k_i^{11} & k_p^{12} k_i^{12} & \dots & k_p^{1n} k_i^{1n} \\ k_p^{21} k_i^{21} & k_p^{22} k_i^{22} & \dots & k_p^{2n} k_i^{2n} \\ \dots & \dots & \dots & \dots \\ k_p^{m1} k_i^{m1} & k_p^{m2} k_i^{m2} & \dots & k_p^{mn} k_i^{mn} \end{bmatrix} \tag{25}$$

Table 1: Parameters of PSO Algorithm

Parameters	Values
Population size	30
No of iterations	100
W_{min}	0.7
W_{max}	0.1
$C_1=C_2$	1.5
Min offset	200

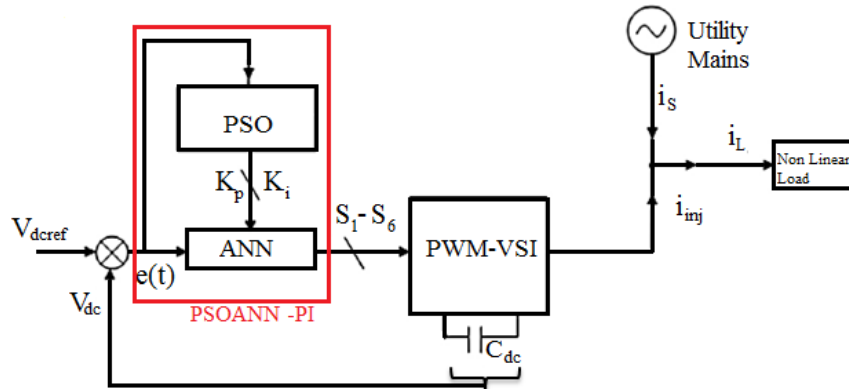


Figure 2: PSOANN tuning Approach for shunt active filter

3.2 Control scheme of ANN

The parameters of proposed algorithm were chosen by off-line assessment using PSO technique. The neural network architecture used in this work is feed-forward network (3 node in the input layer, 20 nodes in the hidden layer, and 1 node in the output layer). The number of hidden layer is decided by the performance optimization of error function and the training period. Cross Validation test is used to validate the selected hidden layers. The hidden layer of the neural network is employing the sigmoid function and shown to be very influential enough to harvest a haphazard mapping among variables. The activation function used at this juncture is the standard sigmoidal function with range between 0 and 1. To train the artificial neural network, a direct learning strategy is employed. Levenberg-Marquardt backpropagation (LMBP) algorithm is used to update the weights of the neural network. The optimized gain parameters are employed as the input of the ANN and the network is trained by Levenberg Marquardt Back Propagation algorithm (LMBP) due to the dynamic response and satisfactory performance. The output of the ANN is employed to provoke the three phase reference currents [Roy, Krishna Mandal, Chandra Mandal et al. (2018)]. LMBP algorithm is apt for the different loading conditions. The algorithm is the combination of Guass newton and Gradient descent methods with advantages of global and local conveyance properties. To avoid overtraining of data, bidirectional recursive neural network is employed for adaptive adjustment of weight through the entire process.

Step 1: According to available information, the network is trained to produce the control pulse (z) with time interval x(t) as the input.

Step 2: The error of the target $x(1), x(2) \dots x(n)$ is determined by the formula

$$\begin{aligned}
 LMBP_{error}^1 &= z(1)^{NN(target)} - z(1)^{NN(out)} \\
 LMBP_{error}^2 &= z(2)^{NN(target)} - z(2)^{NN(out)} \\
 LMBP_{error}^n &= z(n)^{NN(target)} - z(n)^{NN(out)}
 \end{aligned} \tag{26}$$

Step 3: Above equation is engaged to determine the network output,

$$\begin{aligned}
 z(1)^{NN(out)} &= a_1 + \sum_{n=1}^N w_{1n} z(1)^{NN(k)} \\
 z(2)^{NN(out)} &= a_2 + \sum_{n=1}^N w_{1n} z(2)^{NN(k)} \\
 z(n)^{NN(out)} &= a_n + \sum_{n=1}^N w_{1n} z(n)^{NN(k)}
 \end{aligned}
 \tag{27}$$

where a is the node bias function of 1,2, and n.

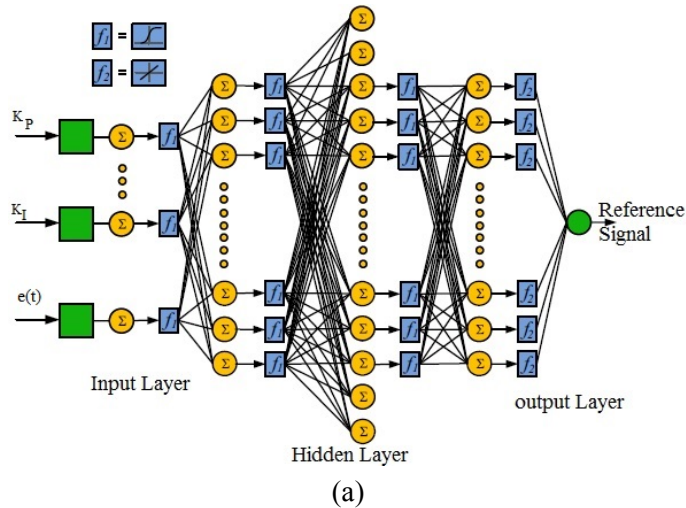
Step 4: The weight of each neuron is computed by $h_{new} = h_{old} + \Delta h$

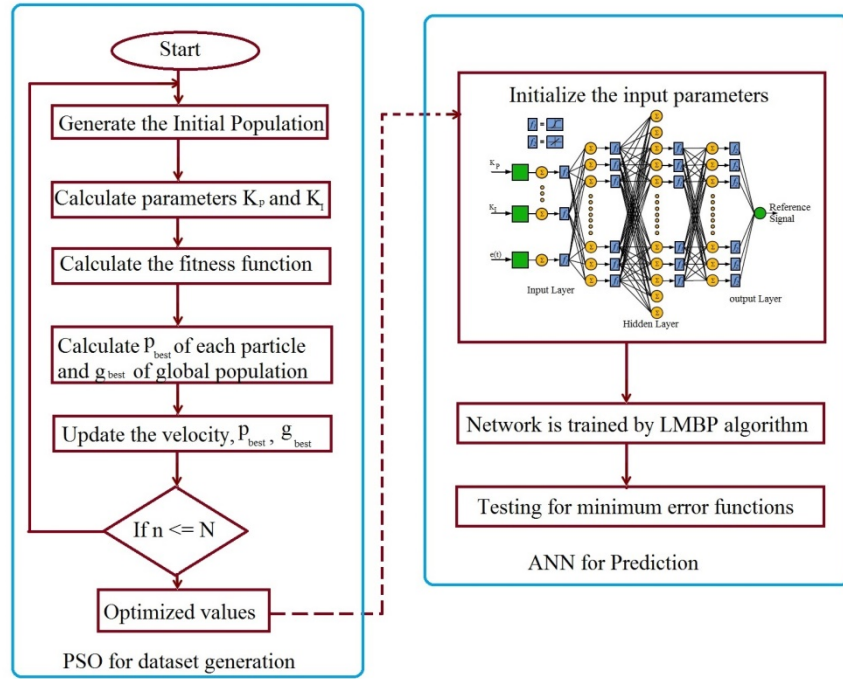
$$\begin{aligned}
 z(1)^{NN(k)} &= \frac{1}{1 + \exp(-h_{1n} z(1) - h_{2n} z(2))} \\
 z(2)^{NN(k)} &= \frac{1}{1 + \exp(-h_{2n} z(2) - h_{nn} z(n))} \\
 z(n)^{NN(k)} &= \frac{1}{1 + \exp(-h_{nn} z(n) - h_{1n} z(1))}
 \end{aligned}
 \tag{28}$$

Step 5: The adjustment of weight is computed by

$$\begin{aligned}
 \Delta h_1 &= L_r \cdot z(1) \cdot LMBP_{error}^1 \\
 \Delta h_2 &= L_r \cdot z(2) \cdot LMBP_{error}^1 \\
 \Delta h_n &= L_r \cdot z(n) \cdot LMBP_{error}^n
 \end{aligned}
 \tag{29}$$

Step 6: Above steps are repeated to minimize the LMBP error (LMBP<0.1).





(b)

Figure 3: (a) Structure of ANN; (b) Flowchart of the PSOANN approach

The successful completion of ANN training, the desired control signal is generated by the shunt active filter. The structure of ANN and flowchart of the proposed control scheme of PSOANN approach is shown in Figs. 3(a) and 3(b).

The performance of the ANN is evaluated by Root Mean Square Error (RMSE), coefficient of determination (R^2) and Mean Absolute Error (MAE)

$$RMSE = \sqrt{\frac{\sum_{i=1}^n (y_{pre,i} - y_i)^2}{n}} \quad (30)$$

$$R^2 = \frac{\sum_{i=1}^n (y_{pre,i} - y_i)^2}{\sum_{i=1}^n (y_{mea,i})^2} \quad (31)$$

$$MAE = \frac{\sum_{i=1}^n |y_{pre,i} - y_i|}{n} \quad (32)$$

Table 2: ANN parameter for the training

Parameters	Values
Input layer	3
Hidden layer	20
Output layer	1
Training function	LMBP
Performance function	Minimized mean square (MSE)
Activation function	Tansig/Tansig/Purelin
Maximum epochs	253
Learning rate L_r	0.04
Performance goal	$1e^{-6}$
Success rate	98.9
Running time	3.08 seconds
RMSE	0.1211
R^2	0.9998
MAE	0.1194

The upper and lower limits of gain parameters are determined as a result of PSOANN approach. The values are denoted in Tab. 3.

Table 3: Decision variables for Gain parameter

Limits	K_p	K_i
Upper	1.48	1.92
Lower	0.04	0.49

4 Results and discussion

An efficient PSO algorithm with ANN based shunt active filter is proposed for the reduction of harmonics in distribution system. Here the proposed system is modelled and simulated in MATLAB/SIMULINK platform. The outcome of the control methodology is validated by utilizing the four test cases with different combination of non-linear loads and also compared with existing methodologies such as PSO, ANN & Conventional PI Controllers. The hardware implementation of the proposed methodology is done using Xilinx Spartan 3E FPGA board. Fig. 4 shows the internal structure of the simulation circuit diagram for proposed optimum controller. The system specification parameters are specified in Tab. 4. For test case 1 to 3, the supply voltage is assumed to be balanced and the supply voltage assumed to be unbalanced in test case 4. The viability of the proposed methodology is illustrated by four test cases which are depicted as follows:

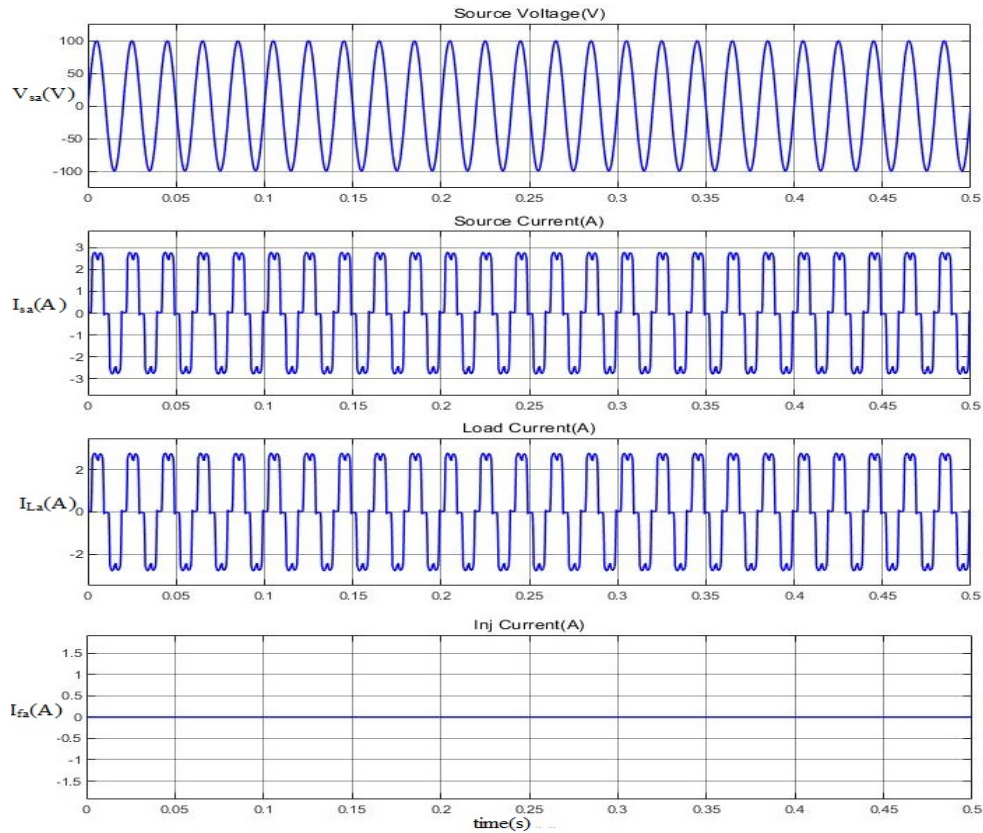


Figure 5: Waveforms of proposed system without SAF

The proposed system is simulated without shunt active filter and the obtained waveform is shown in Fig. 5. The analysis of the test case 1 using balanced supply voltage and three phase rectifier with DC motor is depicted in the Fig. 6, the waveforms of Phase A- V_{sa} , I_{sa} , I_{La} , I_{inj} and V_{dc} is shown respectively. The waveform clearly shows that the load current is highly affected by harmonics due to dc load fed by three phase rectifier, maximum value of THD in the load current is 8.21% in phase A and C, likewise the maximum value of THD in the source current is 0.35 in phase B. The reduction of THD is depending on the injection of the shunt active filter. By that, the stability of the proposed controller is validated by reducing the THD value.

The analysis of the test case 2 using balanced supply voltage and unbalanced RL load is depicted in Fig. 7, the waveforms of phase A - V_{sa} , I_{sa} , I_{La} , I_{inj} and V_{dc} are shown respectively. In this case, maximum value of THD in load current is 1.13% in phase C, likewise the maximum value of THD in the source current is 0.68 in phase A. The suitable current is generated by the SAF and injected in to distribution system to minimize the value of THD. The waveform clearly shows that the source current is balanced and the power factor for phase A is 1 and phase B & C is 0.998.

The Fig. 8 depicts the analysis of the test case 3 using balanced supply voltage and combination of test case 1 and 2, also it shows the waveforms of phase A - V_{sa} , I_{sa} , I_{La} , I_{inj}

and V_{dc} . This case clearly shows that the phase A has 0.86% of maximum value of THD in source current and the phase B has 1.64 as the maximum value of THD in the load current. The power factor for phase A is 0.999, phase B is 0.996 and phase C is 0.998.

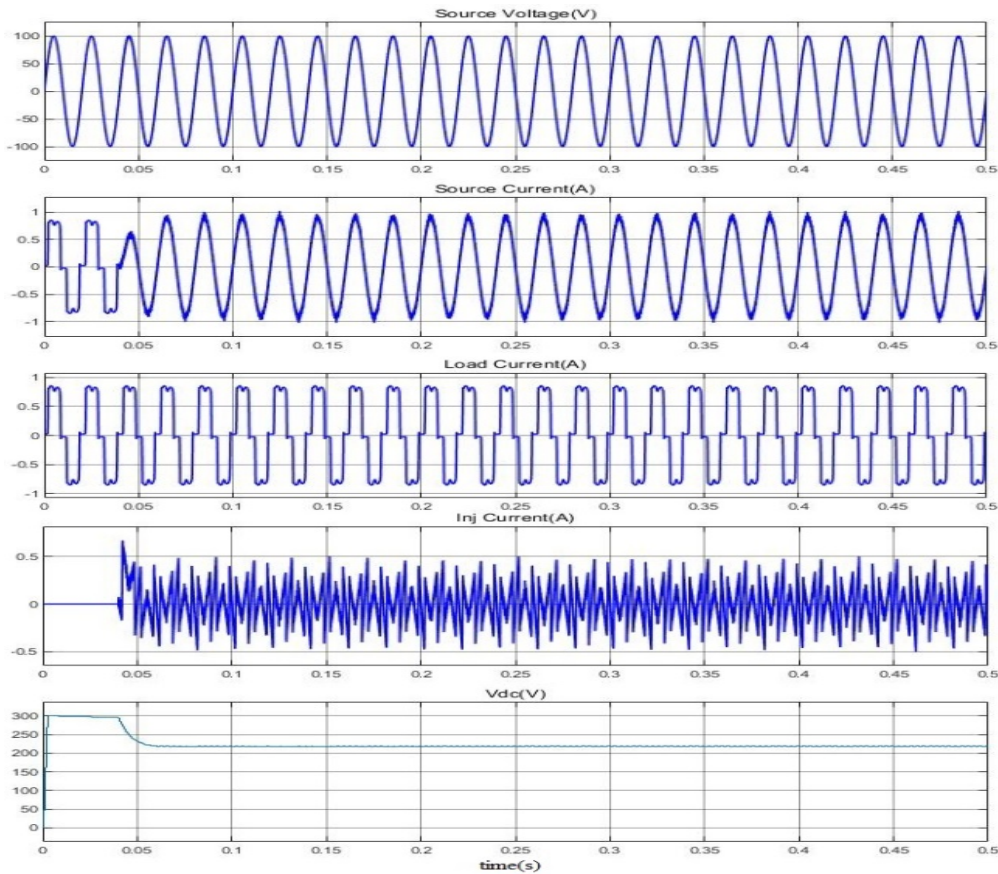


Figure 6: $V_a(V)$, $I_{sa}(A)$, $I_{La}(A)$, $I_{inj}(A)$, $V_{dc}(V)$ of PSOANN-PI Controller for test case 1

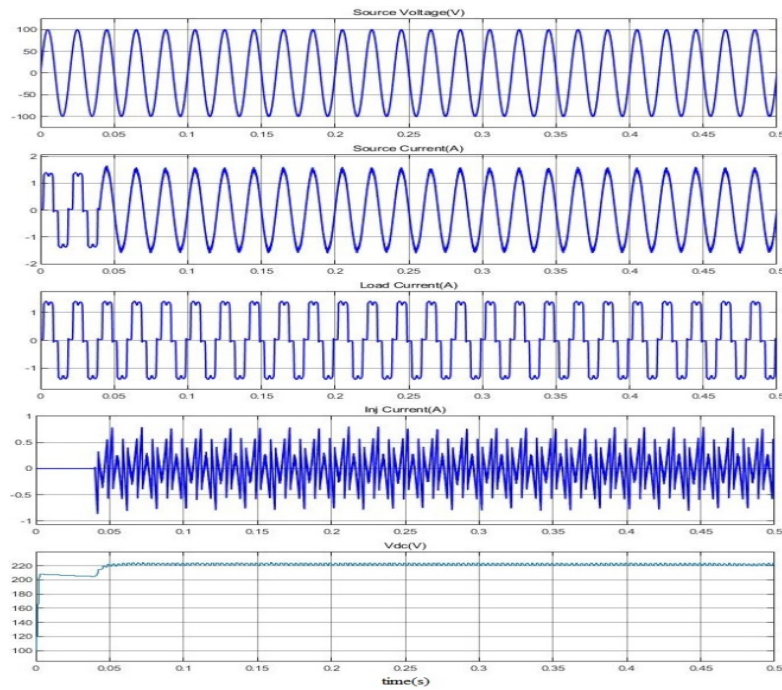


Figure 7: $V_a(V)$, $I_{sa}(A)$, $I_{La}(A)$, $I_{Inj}(A)$, $V_{dc}(V)$ of PSOANN-PI Controller for test case 2

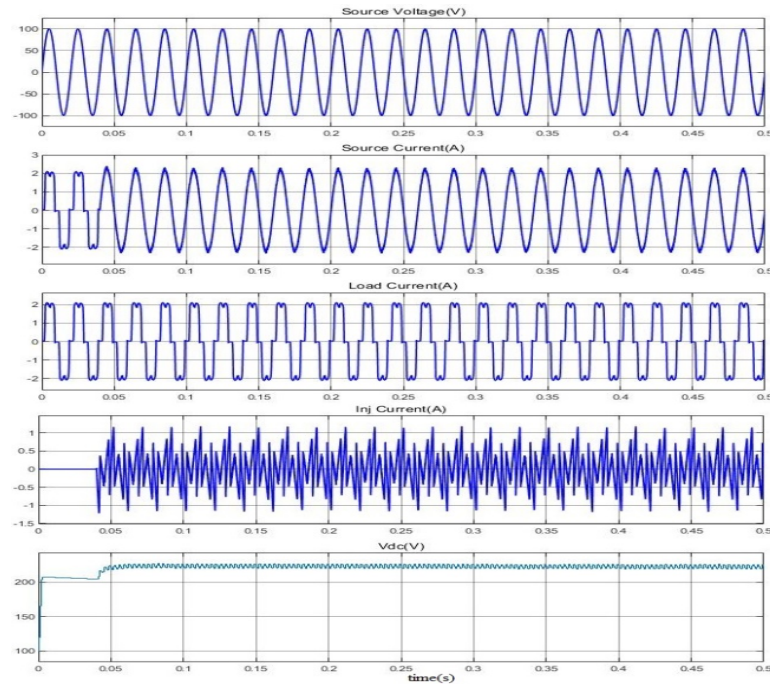


Figure 8: $V_a(V)$, $I_{sa}(A)$, $I_{La}(A)$, $I_{Inj}(A)$, $V_{dc}(V)$ of PSOANN-PI Controller for test case 3

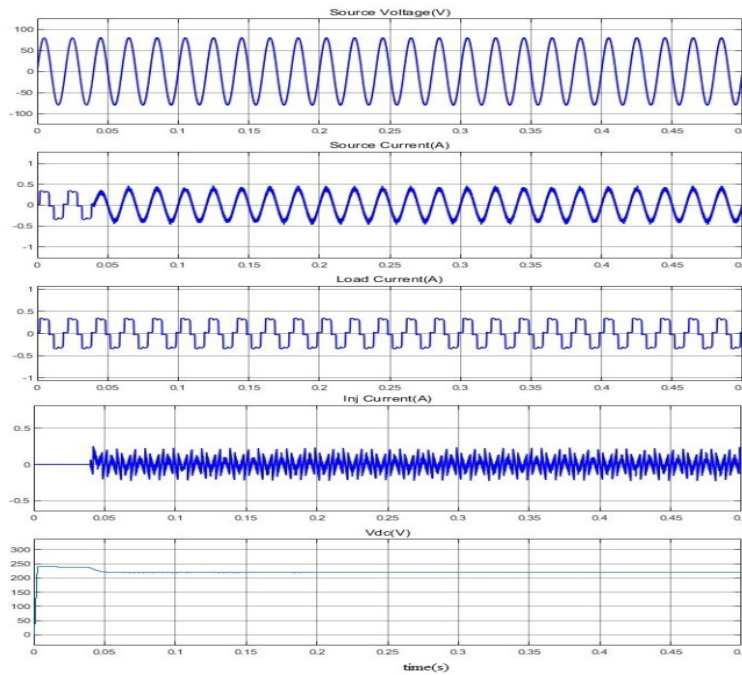


Figure 9: $V_a(V)$, $I_{sa}(A)$, $I_{La}(A)$, $I_{Inj}(A)$, $V_{dc}(V)$ of PSOANN-PI Controller for test case 4

The quick response of dc link voltage for test case from 1 to 4 is depicted in Fig. 10. The proposed PSOANN control algorithm is analyzed by employing different combination of nonlinear loads and it shows that gain parameters are quickly optimized within 0.04 seconds.

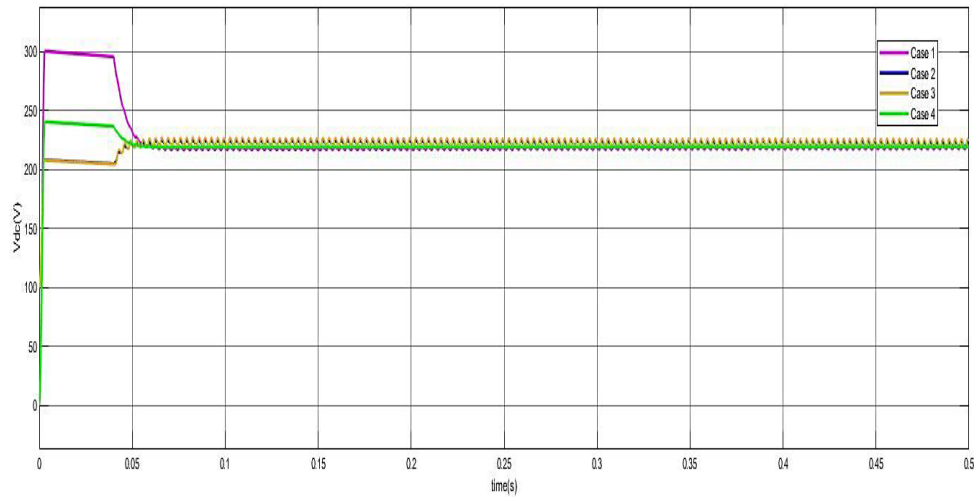


Figure 10: Comparison of dc voltage for various test cases

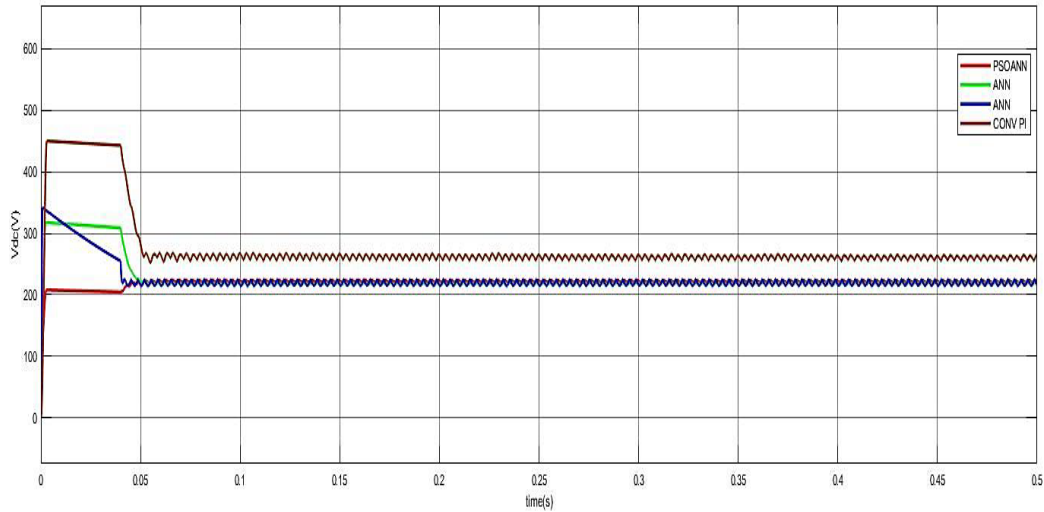


Figure 11: Convergence characteristics of dc voltage for multiple techniques

The convergence characteristic of dc voltage with multiple techniques shows that PSOANN sketches the superior performance in stabilizing the system rapidly shown in Fig. 11. The proposed PSOANN controller shows the settling time more than 8 and 0.2 times for increasing load and more than 11.5 and 0.62 times for decreasing load compared to PSO, ANN and conventional PI controller respectively. It shows that the implementation of PSOANN based estimation of PI controller values is suitable for shunt active filter. Fig. 12 describes the total harmonic distortion value for test case 2.

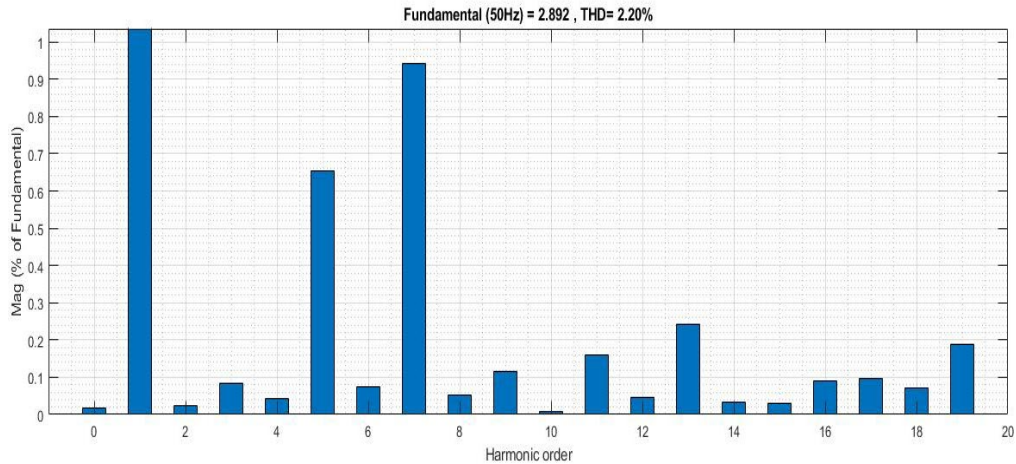


Figure 12: Total harmonic distortion for test case 2

The THD values of test case 1-4, the source and load current for the three phases are clearly depicted in Tab. 5 & Fig. 13. The three phase values of power factors for the test 1-4 is delineated in Tab. 6 & Fig. 14. The optimization parameters using PSOANN is illustrated in the Tab. 7. Tab. 8 & Fig. 15(a) clearly illustrate the comparison of THD

value with existing methods and manifest that PSOANN optimization is superior among all. Fig. 15(b) shows the convergence characteristics of proposed method, case 2 representing the best THD at all iteration are compared with the other methods. The proposed method takes only 15 iterations to obtain the best THD, but the GA, BF and ACO take 22, 30 and 34 iterations, respectively. When compared with other methods, the PSOANN has a better convergence rate as it takes a lower number of iterations to achieve the best solution. The permissible limit of THD is 6.66% for current ratio as per the IEEE 519-2014 Standard 2018 [Mahaboob, Ajithan and Jayaraman (2019)]. The THD values obtained through PSOANN is lower than the current methodologies as per IEEE 519 standard and promising sinusoidal source current.

Table 5: THD Comparison for various techniques

Cases	Method	THD			THD		
		Source Current (%)			Load Current (%)		
		Phase A	Phase B	Phase C	Phase A	Phase B	Phase C
Case 1	PSOANN	0.32	0.35	0.32	8.21	8.20	8.21
	PSO	0.51	0.56	0.59	8.48	8.47	8.48
	ANN	0.66	0.66	0.68	8.52	8.52	8.51
	PI	0.91	0.92	0.91	8.89	8.89	8.90
Case 2	PSOANN	0.68	0.67	0.67	1.12	1.12	1.13
	PSO	0.83	0.82	0.83	1.34	1.34	1.35
	ANN	0.76	0.75	0.75	1.20	1.20	1.21
	PI	1.02	0.89	0.91	1.82	1.92	1.78
Case 3	PSOANN	0.85	0.83	0.86	1.56	1.64	1.59
	PSO	0.94	0.93	0.98	1.81	1.77	1.94
	ANN	0.97	0.96	0.91	1.72	1.81	1.89
	PI	1.20	1.11	1.29	2.54	2.27	2.39
Case 4	PSOANN	1.11	1.02	1.16	5.64	6.12	5.89
	PSO	1.77	1.68	1.89	5.96	6.85	6.67
	ANN	1.72	1.54	1.75	5.81	6.69	6.56
	PI	2.10	2.23	2.17	6.21	6.48	6.37

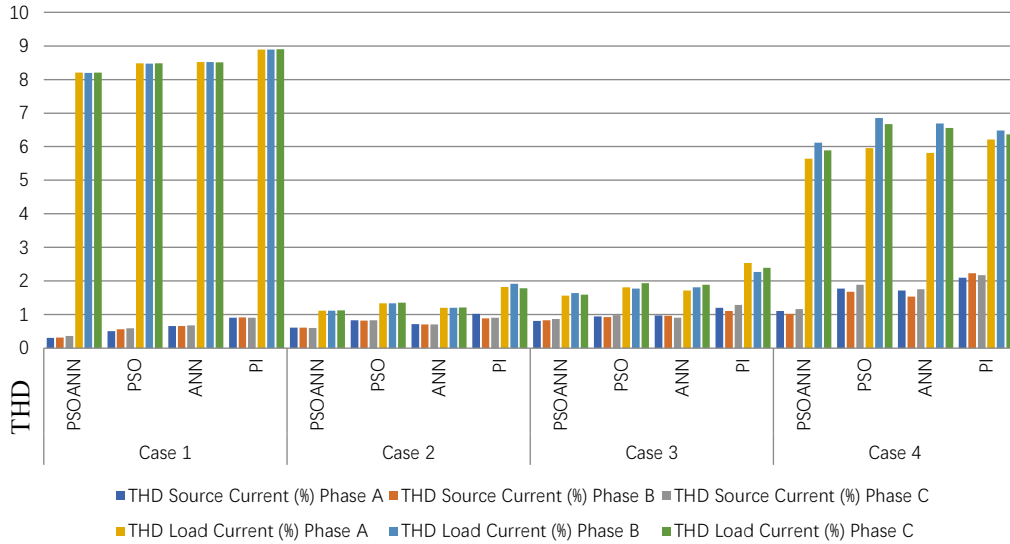


Figure 13: THD Comparison chart for various techniques

Table 6: PF Comparison for various techniques

Cases	Method	Power Factor		
		Phase A	Phase B	Phase C
Case 1	PSOANN	0.999	1	0.997
	PSO	0.956	1	1
	ANN	1	1	0.968
	PI	0.956	1	0.956
Case 2	PSOANN	1	0.998	0.998
	PSO	1	0.998	0.991
	ANN	1	0.998	0.993
	PI	1	0.998	0.997
Case 3	PSOANN	0.999	0.996	0.998
	PSO	0.967	0.996	0.991
	ANN	0.999	0.992	0.997
	PI	0.947	1	0.952
Case 4	PSOANN	1	0.998	1
	PSO	1	0.963	1
	ANN	1	0.943	1
	PI	0.995	0.991	1

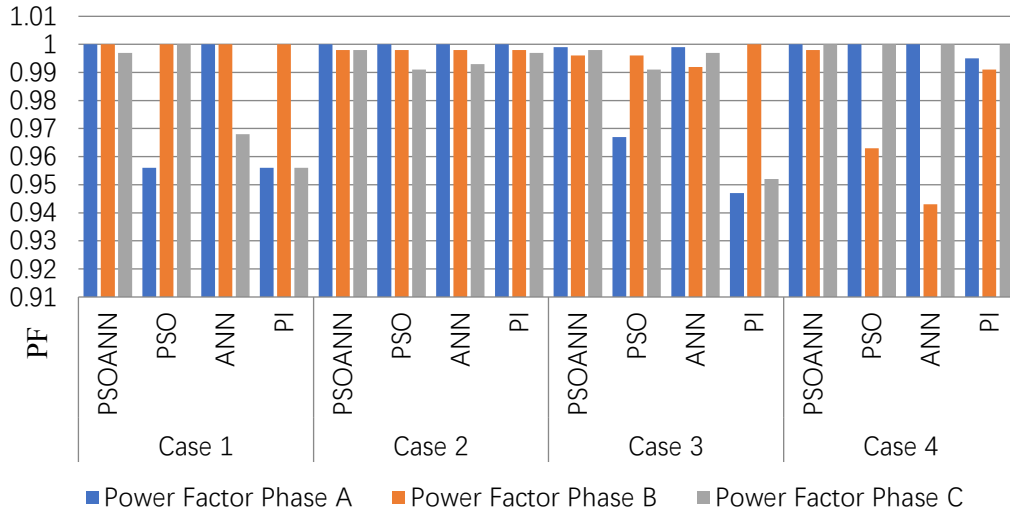


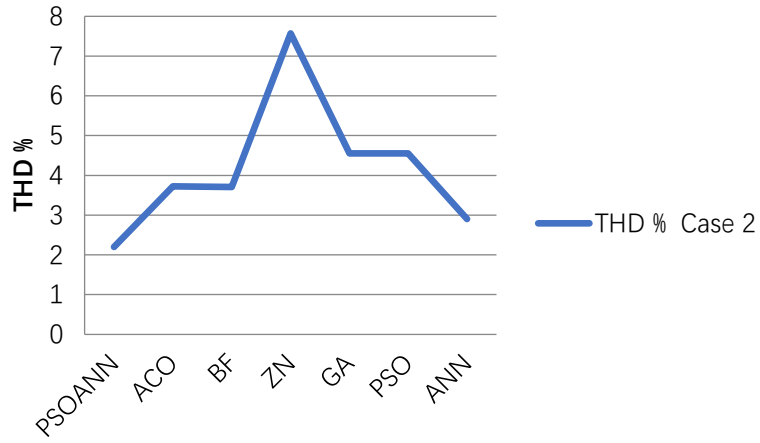
Figure 14: Power factor comparison chart for various techniques

Table 7: Comparison of PI values

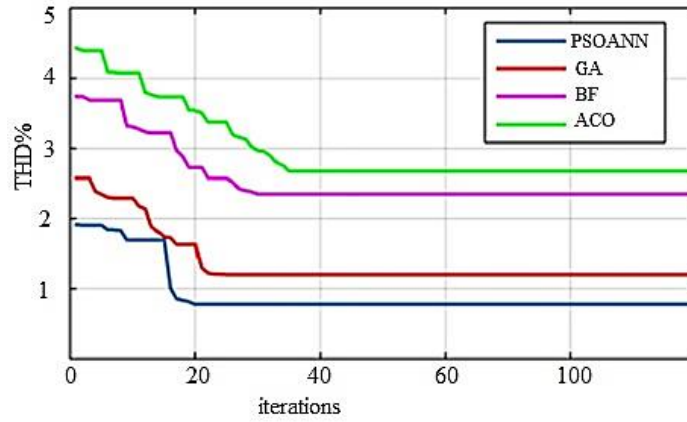
Methods	K_p	K_I
PSOANN	0.1	1
PSO	1.24	1.73
ANN	0.82	1.2
Conventional PI	1	1

Table 8: Comparison of THD with other techniques

Solution techniques	THD % (Test case 2)
PSOANN	2.2
PSO	4.55
ANN	2.9
ACO [Sakthivel, Vijayakumar, Senthilkumar et al. (2015)]	3.72
BF [Mohammadi (2015)]	3.71
ZN [Parithimar Kalaignan (2015)]	7.57
GA [Parithimar Kalaignan (2015)]	4.55



(a)



(b)

Figure 15: (a) Comparison of PSOANN with other techniques; (b) Convergence rate vs. iteration comparison with other methods

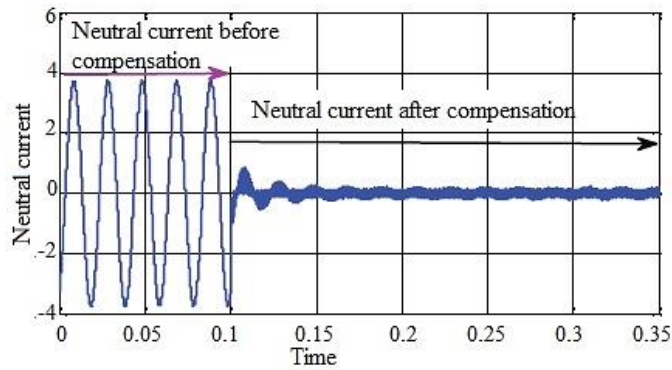


Figure 16: Neutral current before and after compensation

The performance of shunt active filter is captivated by measuring the neutral current shown in Fig. 16. After the gating pulse is applied to the VSI, the neutral current becomes zero. It is due to adjustable nature of neural network.

A laboratory prototype is implemented to validate the shunt active filter with PSOANN based PI control algorithm using Xilinx Spartan 3E FPGA board depicted in Fig. 16. The switching of voltage source inverter for SAF is performed using PWM, which controls the source current.

The experimental results are delineated for the control of DC link voltages under various load current variations. Fig. 17 shows the laboratory prototype system parameters. The control of SAF is implemented through proposed algorithm using space vector pulse width modulation method and it is employed to switching the VSI of shunt active filter, which controls the source current (I_s) to follow the derived value of reference source current (I_s^*). The three-phase source currents are predicted using current transformers (CTs), three-phase source voltage and DC link voltage are predicted using voltage transducer. The predicted signals are conveyed to the ADC card of FPGA board. The three phase unit vector template is generated with help of three phase source voltage. The reference value is compared with the actual value of DC link voltage and the generated error signal is handled through proposed controller. In order to generate the reference source current, peak value of the source current is multiplied by unit vector template. The VSI switching signals are generated by using proposed control algorithm based reference current extraction and space vector pulse width modulation. These switching signals are used to perceive the Shunt active filter.

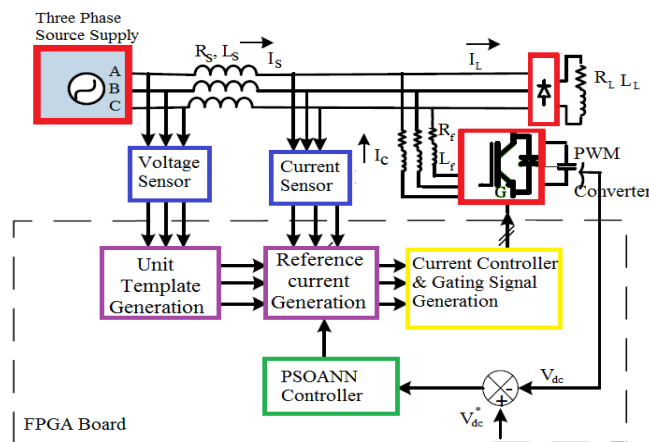


Figure 17: Experimental prototype

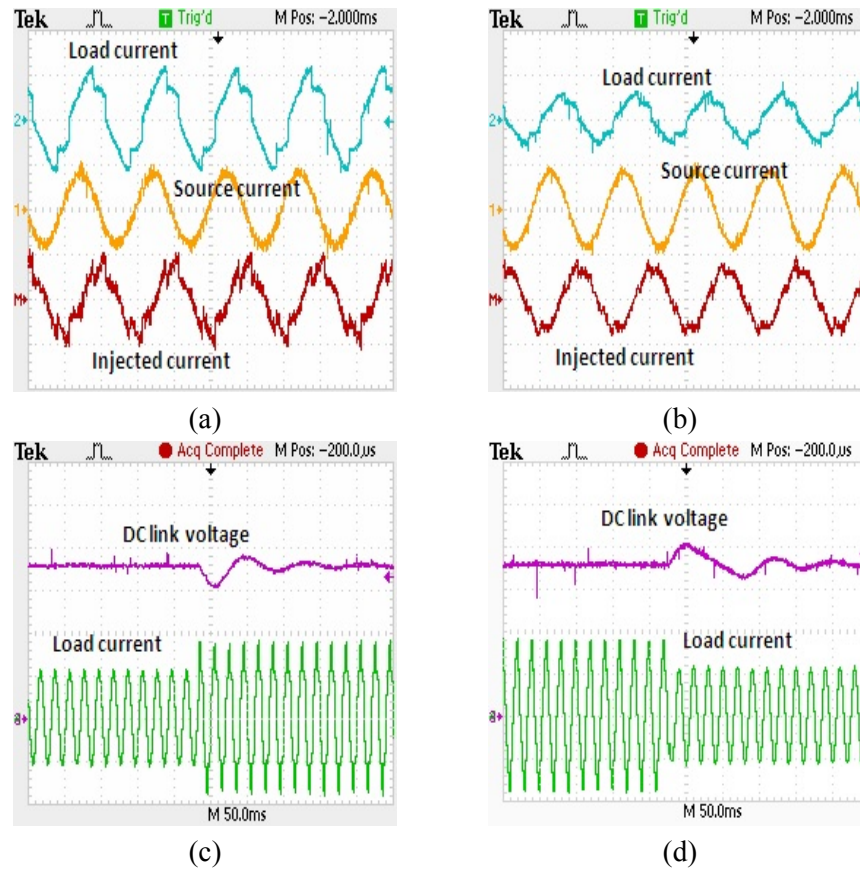


Figure 18: Experimental results for increasing and decreasing DC link voltage for two different load conditions (Phase A-RMS voltage of 100 V/div, RMS Supply current of 2 A/div, time 10 ms/div & V_{dc} -200 V/div, time-200 m/sec)

Figs. 18(a) & 18(b) depicts the load current before compensation, source current after compensation, and injected current under the increasing of load current. Figs. 18(c) & 18(d) depicts the load current before compensation, source current after compensation, and injected current under the decreasing of load current.

The effectiveness of the proposed control algorithm has shown in figures. The Fig. 19(a) depicts the source voltage and current before compensation in phase A and the Fig. 18(b) shows after compensation waveform in phase A.

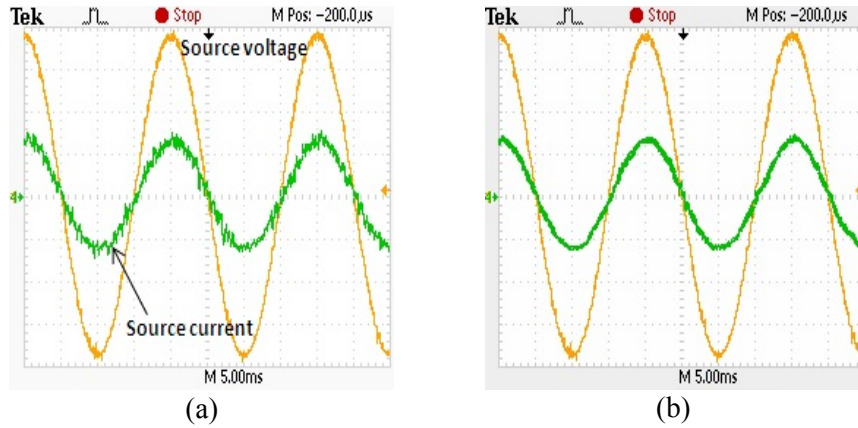


Figure 19: Before and after compensation

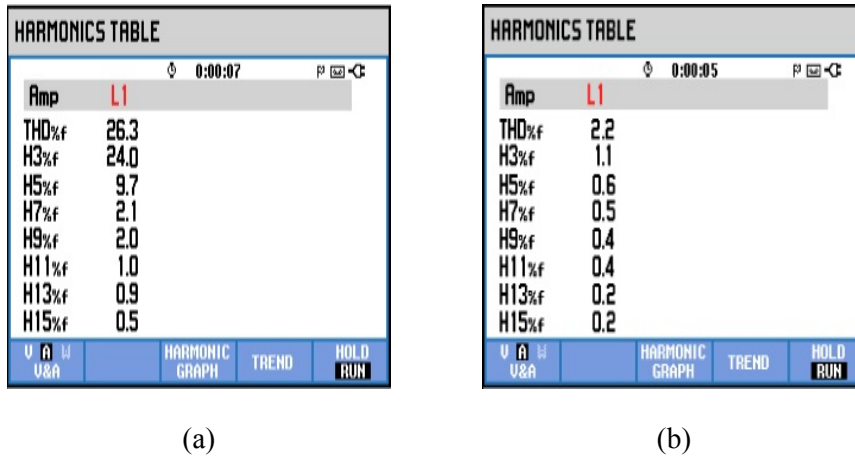


Figure 20: THD value before and after compensation

Fig. 20 clearly shows that the total harmonic distortion (THD) of I_s before compensation is 26.3% and later it has reduced to 2.2% after compensation. It will show the superior performance of the control algorithm employed in the shunt active filter.

5 Conclusion

In this paper, the control algorithm of PSOANN is proposed for the SAF, to reduce the total harmonic distortion in the source side of the distribution system. The PSOANN techniques are employed to find the lower and upper bound values of the PI controller for the shunt active filter. It is evident that the simulation and experimental result of dc bus voltage response of PSOANN based SAF offers faster convergence rate, high filtering capability and superior performance. The multiple test cases are simulated with balanced and unbalanced voltage supply are illustrated and evident that the value of the THD is reduced for various load conditions. The experimental investigation for the suitability of PSOANN optimized control algorithm has been demonstrated for different load conditions. The result of this investigation is found to be an apt choice for estimating the

gain coefficients of PI control-based Shunt active filter.

Conflicts of Interest: The authors declare that they have no conflicts of interest to report regarding the present study.

References

- Arseneau, R.; Heydt, G. T.; Kempker, M. J.** (1997): Application of IEEE standard 519-1992 harmonic limits for revenue billingmeters. *IEEE Transactions on Power Delivery*, vol. 12, no. 1, pp. 346-353.
- Baghaee, H. R.; Mirsalim, M.; Gharehpetian, G. B.; Talebi, H. A.; Niknam Kumle, A.** (2017): A hybrid ANFIS/ABC-based online selective harmonic elimination switching pattern for cascaded multi-level inverters of microgrids. *IEEE Transactions on Industrial Electronics*, vol. 99, pp. 1-10.
- Barghi Latran, M.; Yoldas, Y.; Teke, A.** (2015): Mitigation of power quality problems using distribution static synchronous compensator: a comprehensive review. *IET Power Electronics*, vol. 8, pp. 1312-1328.
- Barik, A. K.; Das, D. C.** (2018): Expeditious frequency control of solar photovoltaic/biogas/biodiesel generator based isolated renewable microgrid using grasshopper optimisation algorithm. *IET Renewable Power Generation*, vol. 12, no. 14, pp. 1659-1667.
- Biswas, P.; Suganthan, P.; Amaratunga, G.** (2017): Minimizing harmonic distortion in power system with optimal design of hybrid active power filter using differential evolution. *Applied Soft Computing*, vol. 61, pp. 486-496.
- Elsisi, M.; Soliman, M.; Aboeela, M. A. S.; Mansour, W.** (2015): GSA-based design of dual proportional integral load frequency controllers for nonlinear hydrothermal power system. *International Journal of Electrical, Computer, Energetic, Electronic and Communication Engineering*, vol. 9, no. 8, pp. 928-934.
- Jain, S.; Agarwal, S.; Jain, A.; Palwalia, D. K.** (2016): Applied precise multivariable control theory on shunt dynamic power filter using sliding mode controller. *IEEE 1st International Conference on Power Electronics, Intelligent Control and Energy Systems*, pp. 1-4, Delhi, India.
- Lee, T.; Wang, Y.; Li, J.; Guerrero, J.** (2015): Hybrid active filter with variable conductance for harmonic resonance suppression in industrial power systems. *IEEE Transactions on Industrial Electronics*, vol. 62, pp. 746-756.
- Letha, S. S.; Thakur, T.; Kumar, J.** (2016): Harmonic elimination of a photo-voltaic based cascaded H-bridge multilevel inverter using PSO (particle swarm optimization) for induction motor drive. *Energy*, vol. 107, pp. 335-346.
- Mahaboob, S.; Ajithan, S. K.; Jayaraman, S.** (2019): Optimal design of shunt active power filter for power quality enhancement using predator-prey based firefly optimization. *Swarm and Evolutionary Computation*, vol. 44, pp. 522-533.
- Marzoughi, A.; Imaneini, H.; Moeini, A.** (2013): An optimal selective harmonic mitigation technique for high power converters. *International Journal of Electrical Power & Energy Systems*, vol. 49, pp. 34-39.

Mikkili, S.; Panda, A. (2012): Simulation and real-time implementation of shunt active filter id-iq control strategy for mitigation of harmonics with different fuzzy membership functions. *IET Power Electronics*, vol. 5, no. 9, pp. 1856-1872.

Mohammadi, M. (2015): Bacterial foraging optimization and adaptive version for economically optimum sitting, sizing and harmonic tuning orders setting of LC harmonic passive power filters in radial distribution systems with linear and nonlinear loads. *Applied Soft Computing*, vol. 29, pp. 345-356.

Panda, A.; Mikkili, S. (2013): FLC based shunt active filter (p-q and I_d - I_q) control strategies for mitigation of harmonics with different fuzzy MFs using MATLAB and real-time digital simulator. *International Journal of Electrical Power & Energy Systems*, vol. 47, pp. 313-336.

Parithimar Kalaignan, T. (2015): *Power Quality Enhancement by Minimizing Current Harmonics Using Soft Computing Based Shunt Active and Hybrid Filters (Ph.D. Thesis)*. Anna University, Chennai, India.

Patel, R.; Panda, A. (2014): Real time implementation of PI and fuzzy logic controller based 3-phase 4-wire interleaved buck active power filter for mitigation of harmonics with id-iq control strategy. *International Journal of Electrical Power & Energy Systems*, vol. 59, pp. 66-78.

Patjoshi, R. K.; Kanta Mahapatra, K. (2013): Performance analysis of shunt active power filter using PLL based control algorithms under distorted supply condition. *IEEE Students Conference on Engineering and Systems*, pp. 12-14, Allahabad, India.

Roy, K.; Krishna Mandal, K.; Chandra Mandal, A.; Narayan Patra, S. (2018): Analysis of energy management in micro grid: a hybrid BFOA and ANN approach. *Renewable and Sustainable Energy Reviews*, vol. 82, 42964308.

Sakthivel, A.; Vijayakumar, P.; Senthilkumar, A.; Lakshminarasimman, L.; Paramasivam, S. (2015): Experimental investigations on ant colony optimized PI control algorithm for shunt active power filter to improve power quality. *Control Engineering Practice*, vol. 42, pp. 153-169.

Suresh, D.; Singh, S. P. (2014): Performance investigation of the shunt active power filter using neural network. *IEEE Students' Conference on Electrical, Electronics and Computer Science*, pp. 1-5, Bhopal, India.

Terciyanlı, A.; Avci, T.; Yilmaz, I.; Ermis, C.; Kose, K. et al. (2012): A current source converter-based active power filter for mitigation of harmonics at the interface of distribution and transmission systems. *IEEE Transactions of industrial Applications*, vol. 48, no. 4, pp. 1374-1386.

Usman, H.; Musa, S. (2013): Harmonic mitigation using single phase shunt active power filter with fuzzy logic controller for the improvement of power quality. *International Journal of Electrical Components & Sustainable Energy*, vol. 1, pp. 29-33.

Yin, X. X.; Lin, Y. G.; Li, W.; Gu, Y. J.; Liu, H. W. et al. (2015): A novel fuzzy integral sliding mode current control strategy for maximizing wind power extraction and eliminating voltage harmonics. *Energy*, vol. 85, pp. 677-686.

Appendix A. Nomenclature

V_{S1}, V_{S2}, V_{S3}	Source voltage
I_{S1}, I_{S2}, I_{S3}	Source currents
V_{My}	phase voltage
V_{sy}	Source voltage
y	denotes the phase
L_{HF}, R_{HF}, C_{RF}	equivalent parameters values of harmonic filters
I_{FC}	Filter current
V_{dc}	DC link capacitor voltage
I_{dc}	Capacitor current
C_{dc}	Shunt Capacitor
V_{NF}	voltage between the neutral and active filter
C_s	switching functions
S_s and S_s'	Switches of the inverter
q_{my}	phase(y) and the switching function
V_s^*	Reference voltage
I_d, I_q	Reference current (direct axis and quadrature axis)
V_{CHFd}, V_{CHFq}	Reference voltage across the filter
k_v	Gain parameter
N	No of particles in the group
D	Dimensions
T	iterations
$v_{k,m}^{(t+1)}$	Velocity of each particle k at iteration t
c_1, c_2	Acceleration constant
$\text{rand}()$	Random number between 0 and 1
V_{kd}	Current position of particle at each iteration
P_{bestk}	Best previous position of k^{th} particle
G_{bestk}	Best particle in global population
$z(n)^{NN(\text{out})}$	Network current output
$z(n)^{NN(\text{tar})}$	Target value of each node
Δh	Change in weight with reference to each output
N	No of data sample
$y_{\text{pre},i}$	Predicted value
$y_{\text{mea},i}$	Measured value
y_i	Sample data value